Applied Energy 193 (2017) 60–73

Contents lists available at ScienceDirect

Applied Energy

journal homepage: www.elsevier.com/locate/apenergy

Modelling of temporal and spatial evolution of sulphur oxides and sulphuric acid under large, two-stroke marine engine-like conditions using integrated CFD-chemical kinetics

Kar Mun Pang [a,*], Nikolas Karvounis [a], Jens Honore Walther [a,b], Jesper Schramm [a], Peter Glarborg [c], Stefan Mayer [d]

[a] Department of Mechanical Engineering, Technical University of Denmark, Nils Koppels Allé, 2800 Kgs. Lyngby, Denmark
[b] Chair of Computational Science, ETH Zürich, Clausiusstrasse 33, ETH-Zentrum, CLT F 11, CH-8092 Zürich, Switzerland
[c] Department of Chemical and Biochemical Engineering, Technical University of Denmark, Søltofts Plads, 2800 Kgs. Lyngby, Denmark
[d] MAN Diesel & Turbo SE, Teglholmsgade 41, 2450 Copenhagen SV, Denmark

HIGHLIGHTS

- A reduced sulphur mechanism, consisting of 4 species and 5 reactions is developed.
- SO_2 to SO_3 conversion and sulphuric acid formation in a marine engine are simulated.
- The conversion at varying fuel sulphur contents and engine conditions is predicted.
- The absolute values of simulated and measured SO_2 to SO_3 conversion levels are close.
- Sulphur acid condensation may begin early at the top part of the cylinder liner.

ARTICLE INFO

Article history:
Received 20 September 2016
Received in revised form 27 January 2017
Accepted 8 February 2017

Keywords:
Combustion
Heavy fuel oil
Sulphuric oxides
Sulphuric acid
Marine engine

ABSTRACT

In this work, three-dimensional computational fluid dynamics (CFD) studies of sulphur oxides (SO_x) and sulphuric acid (H_2SO_4) formation processes in a large, low speed two-stroke marine diesel engine are carried out. The current numerical study aims to investigate the conversion of sulphuric dioxide (SO_2) to sulphuric trioxide (SO_3) and the possibility of H_2SO_4 condensation which are the prerequisites to better understand the corrosion-induced wear phenomenon. This is achieved with the aid of the implementation of a multicomponent surrogate model, which comprises a skeletal *n*-heptane mechanism and a reduced sulphur subset mechanism. In the present work, performance of the coupled CFD-chemical kinetic model is evaluated using both qualitative and quantitative methods. The modelling results show that the temporal and spatial evolutions of SO_x predicted by the skeletal model are similar to those by the base mechanism. Predictions of the variations of SO_x and the associated SO_2 to SO_3 conversion in response to the change of fuel sulphur content, swirl velocity, start of injection, scavenge pressure and humidity qualitatively agree with numerical and experimental results from the literature. The model is further evaluated using the measured SO_2 to SO_3 conversion levels in a low load, low scavenge pressure case and a low load, high scavenge pressure case. The absolute values of simulated and measured conversion levels are close, although the former appear to be higher. The current results show that the flame impinges at the cylinder liner near top dead centre. The gas is cooled rapidly by the wall temperature and H_2SO_4 is produced in the region where the local temperature is less than 600 K. Based on the flue gas correlation, the acid dew point temperature is higher than the wall temperature, suggesting that acid condensation may begin early at the top part of the cylinder liner. The predicted distribution corresponds well with the distribution of corroded parts observed in service engines. The model is expected to serve as an important tool to simulate the rates of SO_2 absorption into lubricating oil film and H_2SO_4 condensation in this combustion system.

* Corresponding author.
E-mail address: kmpan@mek.dtu.dk (K.M. Pang).

http://dx.doi.org/10.1016/j.apenergy.2017.02.020
0306-2619/

1. Introduction

The majority of the world trade is carried out by the international shipping industry. The de-facto standard propulsion technology for large commercial vessels, for instance container ships, bulk carriers and tankers, is the large, low speed two-stroke marine diesel engine. The two-stroke concept offers a thermal efficiency of above 50% despite the fact that the commonly used fuel, heavy fuel oil (HFO), is of low quality. Sulphur is generally present as an impurity in HFO. During the in-cylinder combustion process where air is in excess, most of the sulphur is oxidised to sulphuric dioxide (SO_2). The absorption of SO_2 into the engine lubricating oil film may play a role in cylinder wear [1]. Meanwhile, a fraction of SO_2 is subsequently oxidised to sulphuric trioxide (SO_3) [2] and SO_3 reacts with water vapour (H_2O) to form sulphuric acid vapour (H_2SO_4). The latter condenses as aqueous sulphuric acid on engine cylinder liners where the local temperature is low. This promotes corrosive wear on the cylinder liner. The present solution is to apply lube oil which contains limestone additives to neutralise the acid and hence to impede corrosion on liner surfaces. This however increases the operational costs. Also, the rate of acid condensation is dependent on engine operating conditions and fuel sulphur content. Practical evaluations of acid reaction on cylinder liners are therefore not straightforward and optimising the lube oil treatment becomes complicated. In order to prolong the engine lifespan with minimal expenses on lubrication, an improved understanding of the formation of sulphur oxides (SO_x) in HFO combustion as well as the subsequent H_2SO_4 formation, condensation, and corrosion processes is essential.

While the influences of H_2SO_4 on the physical and chemical behaviour of marine diesel engine lube oils and piston ring were investigated [3,4], engine-out measurements of SO_x from large, low speed two-stroke marine engines, to date, remain rare [5]. The experimental investigations of emissions have been focusing on nitrogen oxides (NO_x) and/or particulate matter [6–9]. Even though Tsukamoto et al. [9] measured the conversion rate of sulphur in fuel to sulfate in particulate matter in their two-stroke marine diesel engine experiment, their study concentrated more on the effects of sulphur on particulate formation but not explicitly the formation of SO_x [9]. The most relevant experimental work was carried out by Cordtz et al. [10] who investigated the tailpipe SO_3 formation of HFO in a medium speed four-stroke test engine. A series of SO_3 measurements were carried out in the exhaust gas produced by a single-cylinder test engine with a rated speed of 1500 revolution per min (rev/min). The measurements covered a range of operating conditions from low to full load under steady-state conditions, wherein start of injection (SOI) timing, engine speed and air-fuel ratio were varied to alter the combustion history. In another study, Engel et al. [11] investigated exhaust gas compositions sampled from five large diesel engines over a range of engine operating conditions using fuels with 0.05–0.8% sulphur. The influences of fuel sulphur contents and engine operating conditions on SO_3 formation were studied. In both studies, variation of the SO_3 production with respect to the change of operating condition and fuel sulphur content was indicated by the conversion of SO_2 to SO_3 (ε), calculated using Eq. (1),

$$\varepsilon = \frac{[SO_3]}{[SO_2] + [SO_3]} \quad (1)$$

This expression assumes the H_2SO_4 concentration is lumped with the SO_3 concentration. Both studies suggested that the conversion levels varied within the range of 1.0–8.0%.

Other investigations on the SO_x formation in marine diesel engines rely mostly on theoretical models [5,12]. For these numerical studies, the fuel oxidation model is different from the typical pure hydrocarbon oxidation model used in gasoline or diesel engine simulations. Instead, accurate high temperature sulphur chemistry is required to be coupled with the fuel oxidation model. Previous research on sulphur kinetics in flames has provided an overall understanding of the general aspects of the associated high temperature chemistry [13–17]. However, early models suffered from a lack of accurate thermodynamics and kinetic data. Glarborg and co-workers [2,16,17] proposed a detailed hydrogen/sulphur/oxygen (H/S/O) reaction mechanism, using laboratory reactor experiments and theoretical predictions to support the model formulation. Although the validation of the H/S/O mechanism was carried out under atmospheric pressure, it would be expected to extrapolate well to higher pressure levels. Cordtz et al. [5] as well as Andreasen and Mayer [12] combined the mechanism with a multi-zone model for the investigation of SO_x formation under large, two-stroke marine diesel engine conditions. In their work, the mechanism did not account for the decomposition or oxidation of hydrocarbons. Solely the post flame phenomena were simulated and chemical reactions were initiated by equilibrating the species at stoichiometric conditions. One of the main limitations of these studies [5,12] or in general multi-zone models [18] was the absence of detailed information of the temperature and combustion product distributions. In addition to this, a mixing constant had to be calibrated for different engine speeds [5].

Alternatively, three dimensional (3-D) computational fluid dynamics (CFD) modelling of marine engines is a promising tool to provide a more comprehensive insight into in-cylinder events [19,20]. Nonetheless, several issues have to be addressed beforehand. First of all, the simulation has to initiate from fuel injection, followed by fuel evaporation, ignition and combustion. An accurate yet compact surrogate model which describes both hydrocarbon and sulphur oxidation has to be constructed. It is noteworthy that, although different reduced mechanisms for sulphur oxidation have been proposed [5,21], they are not coupled with hydrocarbon subsets or validated under engine-like conditions. Another challenge is to simulate the thermal boundary layers on the cylinder wall liner during the high temperature flame jet impingement where the temperature gradient is usually steep [22,23]. The peak temperature in the flame jet can reach above 2700 K while the cylinder liner wall temperature is much lower at approximately 400 K [19]. Based on the steady-state Reynolds-averaged Navier–Stokes (RANS) simulation on heat transfer from combustion gaseous to the piston surface in a large marine engine performed by Jensen and Walther [24], it was found that both the magnitude and the distribution of the predicted wall heat transfer varied significantly when different wall models were applied. This indicates that such calculation was strongly dependent on the empirical models. The local temperature near the cold wall is however crucial for the computation of H_2SO_4 formation rates and has to be properly simulated.

Set against these backgrounds, the objective of this work is to develop numerical models for the investigation of SO_x and H_2SO_4 formation in a large, low-speed two-stroke marine engine. As aforementioned, a compact multicomponent surrogate model that accounts for SO_x formation is not available from the literature. A reduced sulphur subset mechanism is first developed in the current work and is incorporated with the skeletal *n*-heptane model which was previously built [19]. Apart from this, the near wall spatial resolution is also carefully examined to ensure that the thermal boundary layers along the cylinder liner are properly resolved. The coupled CFD-chemical kinetic model is then evaluated using both qualitative and quantitative methods. Finally, temporal and spatial distributions of SO_2 and H_2SO_4 on the cylinder liner are investigated using the model.

The remainder of the paper is structured such that the formulation of the skeletal chemical mechanism and CFD models are next

detailed. This is followed by the descriptions of the mesh configuration and initial conditions. The subsequent section of the paper outlines the comparison of the skeletal model and its base counterpart. In the consequent sections, model evaluation and numerical analyses of the in-cylinder events are presented. Key conclusions from the work are highlighted in the final section of the paper.

2. Numerical formulation and setup

2.1. Chemical kinetic mechanisms

In the development of the multicomponent surrogate model, the 30 species *n*-heptane model employed in the previous work [19] is used to describe the hydrocarbon oxidation in the HFO combustion. Radicals such as hydroxyl (OH), hydrogen atom (H) and oxygen atom (O), which are essential for the calculation of SO_x formation rates, are included. The sulphur chemistry is drawn from Hindiyarti et al. [16]. This subset, which comprises 18 species and 98 reactions, is coupled with the *n*-heptane model. In addition, a reaction (R6), which describes the H_2SO_4 formation from SO_3 and H_2O, is taken into account [5,25]. The rate constant for reaction (R6), k_6 was obtained at 298 K. A more accurate representation of the reaction is $SO_3 + H_2O + H_2O \leftrightarrow H_2SO_4 + H_2O$ with $k_6 = 3.1E{+}07\ \exp(6540/T)$ [26,27] and a sensitivity study on k_6 can be found in Section 3.1.2. The final mechanism consists of 51 species and 169 reactions. This mechanism is henceforth addressed as the full S-HC model for brevity, in which S and HC denote sulphur and hydrocarbon, respectively. It serves as a base model for mechanism reduction and comparison purposes.

A skeletal subset for the sulphur chemistry is developed to reduce the computational costs. As aforementioned, the fuel sulphur is predominantly oxidised to form SO_2 in excess air combustion. In the skeletal model, the oxidation of fuel sulphur to SO_2 is assumed to be fast and irreversible (reaction (R1) in Table 1). To identify the key reactions for SO_3 formation, calculations are conducted for a perfectly stirred reactor (PSR) using CHEMKIN 4.1 [28]. Fixed temperature calculations are conducted at a pressure of 150 bar. Considering that the formation of SO_3 is limited at temperatures of 2000 K and above [5], the tested temperatures are fixed from 1200 K to 1800 K with an interval of 200 K. These are selected to imitate the in-cylinder local temperature during volume expansion after the end of combustion. The PSR simulations are performed for two fuel/air equivalence ratios ($\phi = 0.5$ and 1.0). Rate of production (ROP) analyses are carried out for a residence time of 0.2 s, which is approximately the same order of magnitude as the duration from start of combustion (SOC) to exhaust valve open for the targeted low speed marine engine. The mass fractions of *n*-heptane and sulphur are set to 0.98 and 0.02, respectively.

Fig. 1(a) depicts the ROP results. As seen, under both lean and stoichiometric conditions, the recombination of SO_2 with atomic O (R2) is the controlling reaction for SO_3 formation. The SO_3 decomposition is predominantly governed by $SO_3 + H$ (R3) and $SO_3 + HO_2$ (R5b). Reaction (R5b) forms $HOSO_2$, which serves as an important intermediate species. It is found that the important reactions are similar to those identified by Hindiyarti et al. [16] at lower pressures. The reactions identified here as important constitute the skeletal sulphur subset shown in Table 1. The reaction of SO_2 with HO_2 to form $SO_3 + OH$ is only marginal under the investigated conditions and this step is not included in the skeletal model. Fig. 1(b) compares the SO_3 mole fraction computed using the full and skeletal S-HC mechanisms. As shown, the skeletal model reproduces the SO_3 mole fraction reasonably well under most of the tested conditions.

Based on the assumption that SO_2 formation from fuel sulphur is infinitely fast and irreversible as well as the ROP results, the full sulphur subset mechanism is reduced to 4 species with 5 reactions. With the reduced counterpart, the multicomponent mechanism consists of 37 species with 77 reactions. This is henceforth addressed as the skeletal S-HC model for brevity and its performance is next assessed in 3-D CFD marine engine simulations.

2.2. CFD submodels

The current 3-D CFD simulations are performed in the unsteady RANS framework using the commercial code, STAR-CCM+ version 10 [29]. The Eulerian-Lagrangian framework is utilised to solve the two-phase flow of the fuel spray jet. Rosin–Rammler is applied to model the fuel droplet size distribution while the Kelvin Helmholtz–Rayleigh Taylor (KH–RT) is implemented to simulate the spray breakup. In addition, the Ranz–Marshall correlation is implemented to calculate the droplet heat transfer with the surrounding gas phase. The turbulent flow is modelled using the k–ω SST model. As highlighted in the introduction, both the magnitude and the distribution of the predicted wall heat transfer varied significantly when different wall models were applied [24]. The all y^+ wall model is employed in the current simulations, in which high and low y^+ wall models are determined based on the local y^+ [29]. When the near-wall mesh resolution is not consistent with the modelling assumptions, significant errors can result. Hence, at the vicinity of the cylinder liner where the corrosion-induced

Table 1
Reactions and the Arrhenius parameters of the skeletal sulphur model.

No.	Reaction	A	n	T_a	Reference
1	Fuel-S + $O_2 \rightarrow SO_2$	Global step, fast			Present work
2	$SO_2 + O(+M) \leftrightarrow SO_3(+M)$	3.70E+11	0	850	[16]
	Low-pressure limit	2.40E+27	−3.6	2610	
	Troe parameters 0.442, 316, 7442				
	Low-pressure limit (N_2)	2.90E+27	−3.58	2620	[16]
	Troe parameters (N_2) 0.43, 371, 7442				
3	$SO_3 + H \leftrightarrow SO_2 + OH$	8.40E+09	1.22	1670	[16]
4	$SO_2 + OH(+M) \leftrightarrow HOSO_2(+M)$	5.70E+12	−0.27	0	[16]
	Low-pressure limit	1.70E+27	−4.09	0	[16]
	Troe parameters 0.10 1E−30 1E+30				
	N_2/1/SO_2/5/H_2O/5/				
5	$HOSO_2 + O_2 \leftrightarrow HO_2 + SO_3$	7.80E+11	0	330	[16]
6	$SO_3 + H_2O \leftrightarrow H_2SO_4$	7.23E+08	0	0	[5,25]

Note: A, n and T_a represent the pre-exponential factor, the temperature exponent and the activation temperature in the Arrhenius temperature-dependent form, where $k = AT^n exp(-T_a/T)$. The unit of k (and A) is $mol^{1-m}\ cm^{3m-3}\ s^{-1}$, where m is the overall order of the reaction; while T_a is given in K.

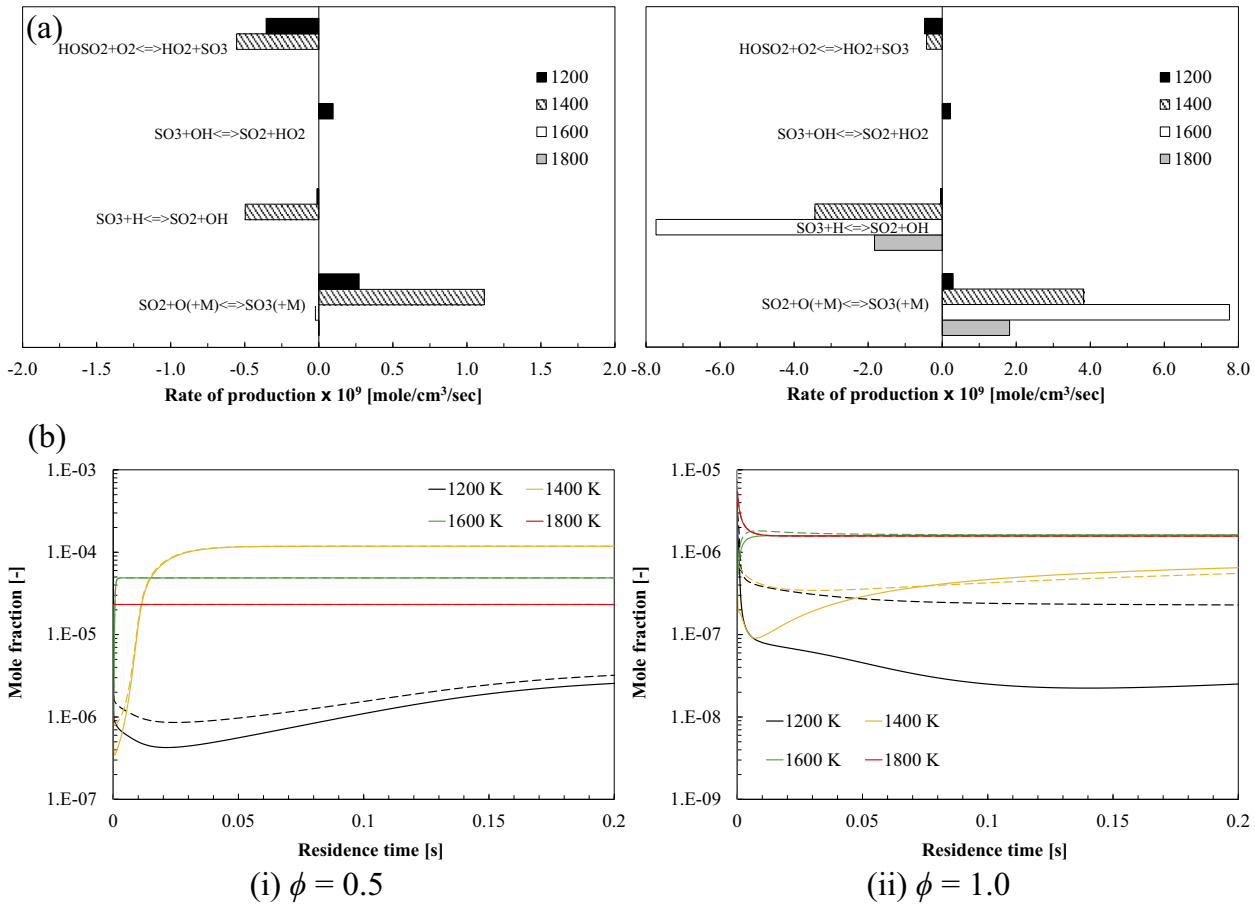

Fig. 1. (a) Rate of production for SO_3 reactions and (b) comparisons of SO_3 mole fraction calculated using the skeletal and full S-HC models at (i) $\phi = 0.5$ and (ii) $\phi = 1.0$ for P = 150 bar. Note for Fig. 1(b): Solid lines represent the skeletal model results while dotted lines denote the full model results.

wear is observed, a sufficiently fine mesh is applied in order to ensure that the y^+ values are around unity [29]. With this, the low y^+ wall model is used to directly resolve the associated viscous sublayer and needs no explicit modelling to predict the flow at the vicinity of the wall boundary. The wall shear stress is computed as in laminar flows [30]. Otherwise, the high y^+ wall model i.e. the classic wall-function approach is used when the local y^+ is higher than 30 [29]. The chemical kinetic mechanisms developed in Section 2.1 are incorporated into the CFD code through the implementation of the DARS-CFD toolkit [29], where the well-stirred reactor (WSR) model is implemented. In turbulent flows, the diffusion process is mainly governed by the turbulent diffusivity. Salvador et al. [31] demonstrated that the evolutions of axial fuel concentration of non-evaporative diesel spray predicted by their model with the range of turbulent Schmidt numbers between 0.5 and 1 were identical. Hence, the default turbulent Schmidt number of 0.9 is used in the simulations. More detailed descriptions on model formulation can be found in the previous work [19].

2.3. Mesh configuration

The simulated engine is the 4T50ME-X test engine at MAN Diesel & Turbo [19,32]. The engine has a cylinder bore and stroke of 0.5 m and 2.2 m, respectively. The cylinder has 30 equally spaced scavenge ports with port angles of 20° with respect to the radial direction. The simulations performed here consider only one engine cylinder and initiate from Top Dead Centre (TDC). Two injectors are fitted at each side in the cylinder and each of the injectors consists of four nozzle holes with diameter of 1.05 mm. The symmetry imposed by the two identical injectors allows a 180° sector mesh to be used to represent half of the combustion

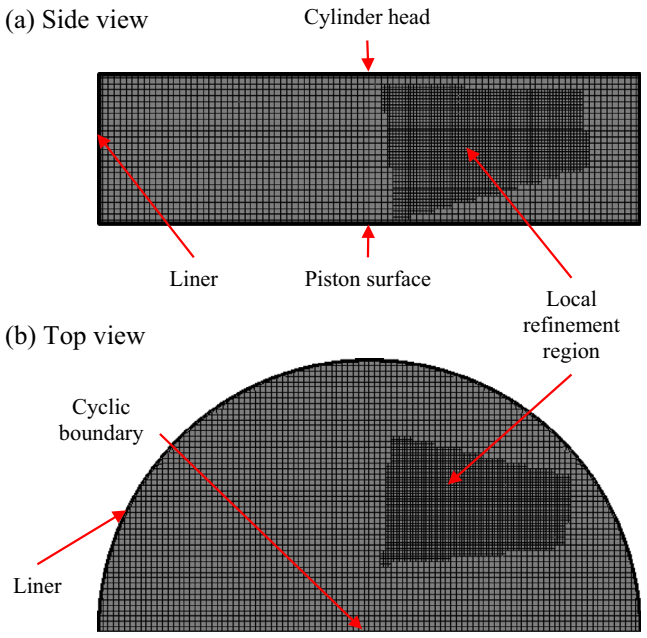

Fig. 2. (a) Side view and (b) top view of the computational grid used in the marine engine simulations. (Adopted from [19]).

chamber. An illustration of the computation grid is provided in Fig. 2 while the main specifications for the test engine and injectors can be found in Table 2.

Lube oil is injected in two-stroke service engines and lube oil films with a thickness of at least a few micrometer are formed to protect the engine liner from corrosion [33]. The H_2SO_4 and/or water vapour condense on the oil films and mix with the lube oil. Meanwhile, the aqueous sulphuric acid reacts with the alkaline in the lube oil [3]. Multicomponent fluid films with complex properties are then formed. Modelling of the fluid films is not taken into consideration in the current simulations since the condensation process and the behaviour of these fluid films are beyond the present scope of work. The design of the mesh configuration is therefore not constrained by the fluid film thickness and is adapted to the predictions of SO_x and H_2SO_4.

The 180° computational grid used in the previous work [19] is set as the reference mesh and the spatial resolution is re-examined. For the reference mesh, the minimum isotropic cell size is 2.5 mm at the vicinity of the injection tip and a larger cell size of 5.0 mm is used in the bulk gas region at TDC. Towards each wall boundary, the mesh resolution is designed to be finer in an exponential manner where cells adjacent to each wall have a thickness of approximately 5.0 μm. The computational grid consists of approximately 290,000 cells [19]. The sensitivity of the spatial resolution is evaluated based on two criteria. The first criterion is the SO_2 to SO_3 conversion up to 90 CAD ATDC while the second is the local cell temperature adjacent to the cylinder liner during flame impingement. For the first criterion, the cell size within the bulk gas region is set to 2.5 mm in all three x-, y- and z-directions. The associated number of cells escalates to approximately 1.35 million. This mesh configuration is used to examine if the temporal evolution of averaged SO_x concentration results reaches grid independence, particularly at later CADs when the mesh is stretched in the axial direction. For the second criterion, twenty prism layers are constructed next to the cylinder liner to resolve the thermal boundary layers. This is essential to improve the prediction of local temperature and H_2SO_4 formation near the liner wall region. The minimum cell thickness is reduced by a factor of ten to 0.5 μm and the total number of cells increases to approximately 410,000. The summary of each mesh configuration can be found in Table 3. The sensitivities of the prediction of SO_2 to SO_3 conversion and local temperature/species formation near the liner wall region to different mesh configuration can be found in Section 3.1.1.

2.4. Initial conditions

The full load case presented in the previous work [19] is set as the reference case, but a fuel sulphur content of 2.0% (by mass) of the total HFO fuel mass delivered is taken into consideration. The engine speed is fixed at 123 rev/min. In the simulated uniflow scavenged large two-stroke marine engine, angled ports near the bottom of the cylinder function to generate swirling flow. At TDC, the maximum tangential velocity ($U_{\theta,max}$) is 21 m/s. The in-cylinder pressure at TDC (P_{TDC}) is set to 152 bar and a total fuel mass (m_{fuel}) of 44.6 g is delivered. The fuel is delivered for a duration of 20.8 crank angle degrees (CADs), where the SOI and end of injection (EOI) are set at 1.2 and 23 CAD after top dead centre (ATDC), respectively. A parametric study is carried out, where only one parameter is varied independently while others are fixed at the values used in the reference case. This is to ensure that the effects on combustion characteristics and SO_2 to SO_3 conversion in response to each variation can be clearly demonstrated.

Table 2
Main specifications for the 4T50ME-X test engine.

Parameter	
Bore (m)	0.5
Stroke (m)	2.2
Connecting rod (m)	2.885
Number of scavenge ports (–)	30
Scavenge port angle (°)	20
Number of injectors (–)	2
Number of nozzle holes of each injector (–)	4
Nozzle hole diameter (mm)	1.05

As shown in Table 4, three different fuel sulphur content levels of 0.5%, 1.0% and 2.0% are investigated. Besides this, the tangential velocity and SOI timing are altered in order to evaluate effects of gas mixing and pressure rise on SO_3 formation, respectively. The pressure at TDC is also changed to investigate the coupling effects from the in-cylinder air mass and peak pressure. This is to imitate different compression pressure attributed by the change of scavenge pressure. The subsequent part of the parametric study varies the initial H_2O composition, with the aim to emulate different humidity levels in the service engine. In the last part, the model is used to simulate the SO_2 to SO_3 conversion in a low load, high scavenge pressure and a low load, low scavenge pressure case. The computed SO_2 to SO_3 conversion in these cases is evaluated using both qualitative and quantitative methods.

3. Results and discussions

3.1. Sensitivity studies

3.1.1. Mesh resolution

The SO_2 to SO_3 conversion illustrated in Fig. 3(a) is computed using Eq. (1). As seen, the conversion level predicted using the reference mesh is close to that of the fine mesh, indicating that the reference mesh reaches grid independence. Next, two test cases with different cylinder liner wall temperatures are used to examine the near wall temperature distribution. Fig. 3(b) provides the temperature distribution along a line probe for a distance of 20 μm from the wall liner at 30 CAD ATDC where the flame impingement is observed. As can be seen, the mesh with ten prism layers is insufficient to resolve the thermal boundary layers. The local temperatures adjacent to the wall are 573 K and 693 K in the cases with wall temperatures of 323 K and 523 K, respectively. With the use of the twenty-prism layer mesh, the local cell temperatures of the cell adjacent to the wall are approximately 353 K and 538 K, respectively. Considering that the temperature gradient is steep at these locations, these values are satisfactorily close to their respective wall temperatures. The highest y^+ value at the cylinder liner remains below 1.9 for the tested conditions. It is concluded that the thermal boundary layers are sufficiently well resolved and the mesh configuration with twenty prism layers is hereafter applied in all the subsequent simulations.

3.1.2. Physical and chemical models

The sensitivity of the turbulence model is evaluated based on SO_x formation in a high load case (baseline) and a low load case (low load, low scavenge pressure). The results can be found in Fig. 4(a). The realizable k-ε model is used as an alternative model here. The SO_2 formation is independent from the turbulence model used. Although the SO_2 to SO_3 conversion is higher with the use of the realizable k-ε model, the percentage point of the conversion remains within 0.6% in both the high and low load cases.

On the other hand, it is noteworthy that the rate constant of reaction (R6) in Table 1 which describes the formation of H_2SO_4 from SO_3 and H_2O was determined at room temperature and pressure. To the authors' knowledge, there are no data available under engine-like conditions. The alternative H_2SO_4 formation reaction as

Table 3
Summary of the mesh configurations investigated in the current work.

Mesh	Isotropic cell size in the spray region (mm)	Isotropic cell size outside the spray region (mm)	Thickness of the cell adjacent to the wall (μm)	Number of prism layers (–)	Total number of cells (–)
I	2.5	5.0	~5.0	10	289,531
II	2.5	2.5	~1.0	10	1,346,347
III	2.5	5.0	~0.5	20	407,247

Table 4
Operating conditions of the test cases.

Fuel sulphur (% by mass)	SOI ATDC (CA°)	P_{TDC} (bar)	Initial H_2O (% by mass)	m_{fuel} (g)	$U_{0,max}$ (m/s)	Engine speed (rev/min)	Engine load
0.5 1.0 2.0[a]	1.2	152	0	44.6	21	123	High
2.0	1.2	152	0	44.6	16 21[a] 26	123	High
2.0	0 1.2[a] 2.4	152	0	44.6	21	123	High
2.0	1.2	147 152[a] 167	0	44.6	21	123	High
2.0	1.2	152	0[a] 0.5 2.0 4.0	44.6	21	123	High
2.0	1.7	67 76	0	19.8 18.9	21	78	Low

[a] Reference case which is the same in all the parametric studies.

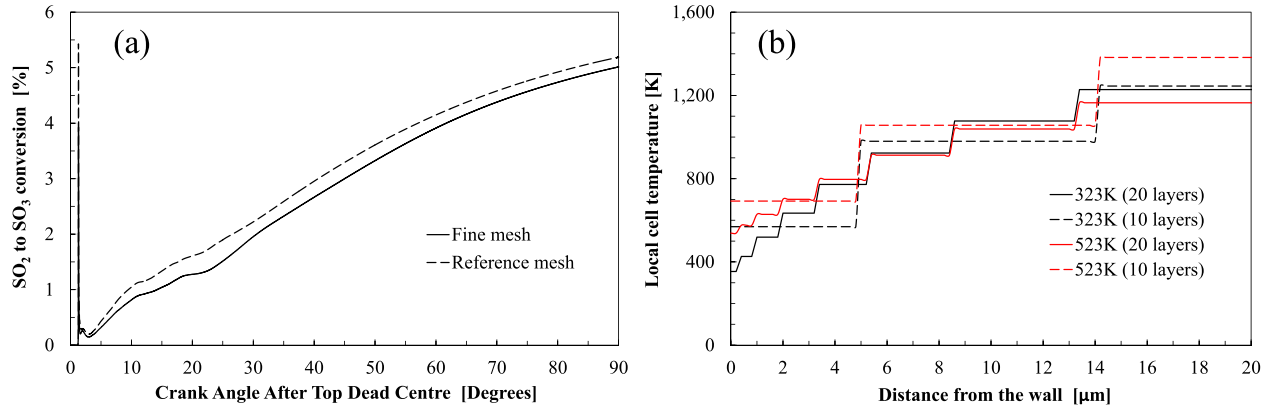

Fig. 3. Comparisons of (a) SO_2 to SO_3 conversion using two different mesh sizes in the bulk gas region and (b) local temperatures using different number of prism layers near the wall region.

proposed in [26,27] is investigated here. Fig. 4(b)(i) shows that the averaged H_2SO_4 concentration predicted by both H_2SO_4 formation reactions have very small differences. The sensitivity study is next extended to high load cases with different initial H_2O levels as depicted in Fig. 4(b)(ii). Similar to the previous observation, the difference is not pronounced. For all the test conditions, the relative difference remains within 5%.

3.2. Comparisons of full and skeletal S-HC models

3.2.1. Spatial evolution

Fig. 5(a)–(d) depicts the distribution of the mass fraction of SO_2 and H_2S on two perpendicular planes created across the spray combustion region at 10 CAD ATDC. As illustrated by Fig. 5(a), SO_2 is the principal SO_x within the flame jet when the skeletal model is applied. Comparisons between Fig. 5(a) and (c) show that spatial distribution of SO_2 predicted using the skeletal and full S-HC models has minor discrepancies. When the latter is used, formation of H_2S dominates at regions with high equivalence ratio i.e. fuel-rich regions (Refer to Fig. 5(e)). The spatial distribution of total SO_2 and H_2S mass fractions shown in Fig. 5(b) is found to be closer to that of SO_2 predicted using the skeletal model. Yet, the associated total mass fraction is lower since the oxidation of fuel sulphur is slower when the finite rate chemistry is used. This is further discussed using the species temporal evolution profiles in Section 3.2.2. Based on the present CFD results, SO_3 is formed at the vicinity of the diffusion flame where atomic O is formed. A further elucidation is provided below.

Fig. 6 demonstrates the distribution of SO_3 mass faction within the temperature-equivalence ratio map. When a noticeable

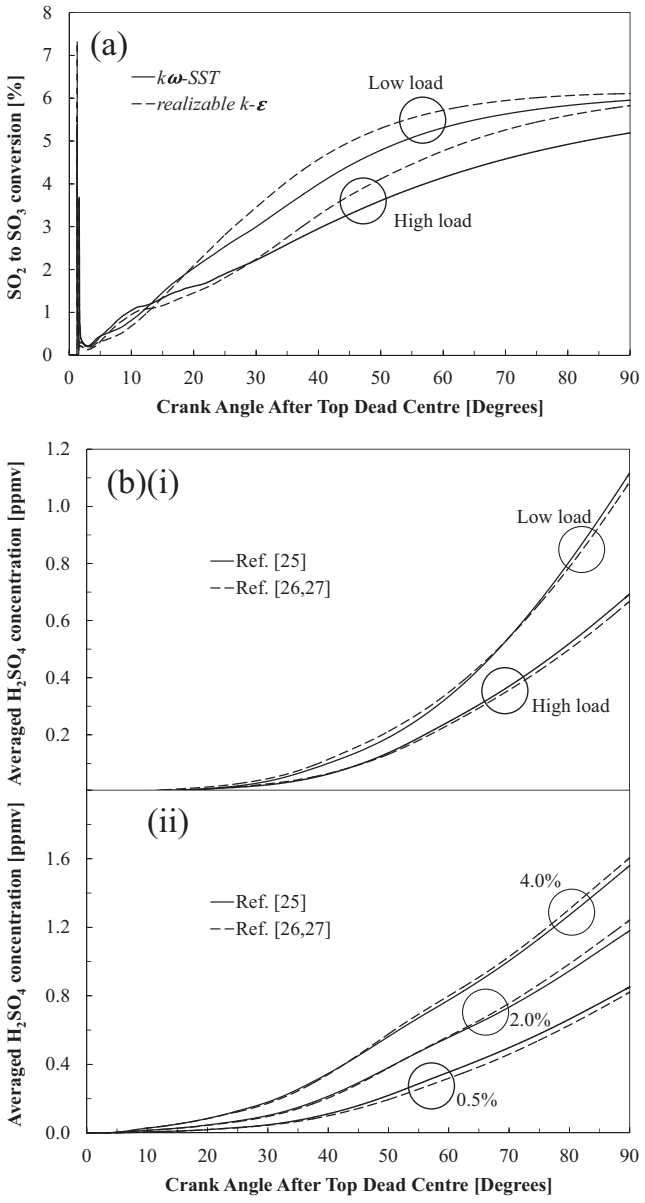

Fig. 4. Comparisons of (a) SO_2 to SO_3 conversion using two different turbulence models at various engine loads and (b) averaged H_2SO_4 concentrations using different rate constants at various (i) engine loads and (ii) initial H_2O levels (by mass).

amount of SO_3 is formed, the flame has impinged at the wall and the SO_3 has also been broadly distributed by convection. In order to provide a clearer illustration, only cells with significant production rate of SO_3 (from SO_2) are plotted. The temperature-equivalence ratio map shows that SO_3 formation is limited above 2000 K. The formation SO_3 is increasingly favoured as the in-cylinder temperature reduces during expansion. As shown in Fig. 6(c)–(d), the primary SO_3 formation takes place within the temperature range from 2000 K to 1200 K. It should also be noted that the SO_3 formation occurs mainly within the stoichiometric and fuel lean regions. The temperature-equivalence ratio maps and SO_3 spatial distributions predicted by the full and skeletal S-HC models are identical. As such, the prediction of H_2SO_4 formation is also expected to be similar when the gas containing H_2O and SO_3 are cooled upon contact with the cylinder wall liner surface.

3.2.2. Temporal evolution at different fuel sulphur levels

The temporal evolutions of averaged SO_x and H_2SO_4 concentrations calculated using the skeletal and full S-HC mechanisms are compared in Fig. 7. When the fast, irreversible reaction is used to describe SO_2 formation from fuel sulphur, the averaged SO_2 concentrations increase at a faster rate. Otherwise, the conversion depends on the overall burning rate. Based on a separate ROP analysis (not shown), the governing species in the oxidation of sulphur to SO_2 include S_2, SH, SO and H_2S, in which H_2S is produced under fuel rich conditions. Fig. 7(a) depicts that as the relevant species and reactions are integrated into the skeletal model, the temporal evolution of SO_2 is akin to the full S-HC results. Fig. 7(a) also demonstrates that the SO_2 produced by the full S-HC model increases almost linearly with the fuel sulphur content. The averaged SO_2 concentrations at 90 CAD ATDC are 119, 243 and 485 ppm by volume (ppmv) for fuel sulphur content of 0.5%, 1.0% and 2.0%, respectively. The averaged SO_2 concentrations at 90 CAD ATDC predicted by the full S-HC model are approximately 6% lower as compared to those calculated using the fast, irreversible reaction in the skeletal model. The difference is caused by the H_2S which is not fully oxidised. As shown earlier in Fig. 5(d), H_2S is produced and starts to dwell on top of the piston surface where the region is fuel rich. Its concentration gradually decreases due to oxidation. However, the oxidation rate of H_2S decreases significantly at approximately 45 CAD ATDC, attributed to the absence of O_2 at the vicinity. Besides this, it is worth mentioning that the WSR model is used in the current simulations, where the sub-grid turbulence chemistry interaction is not accounted for. This may also lead to the rapid consumption of oxidiser in the earlier stage. Hence, a small amount of H_2S is not oxidised and remains until 90 CAD ATDC.

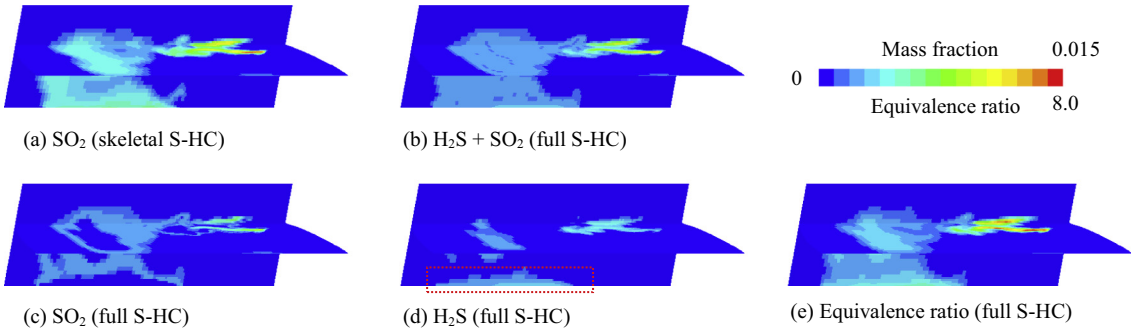

Fig. 5. Distributions of (a)–(d) species mass fraction and (e) equivalence ratio at 10 CAD ATDC.

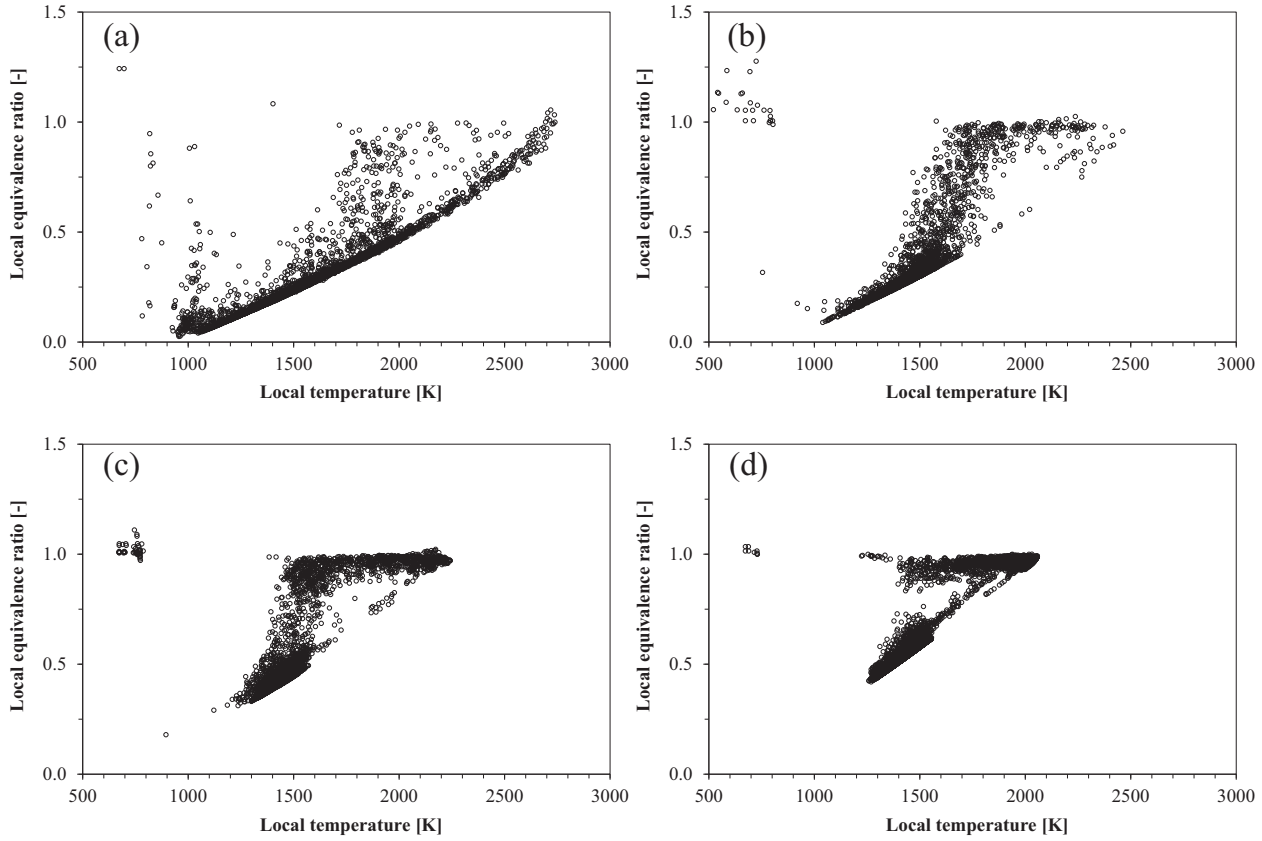

Fig. 6. Local temperature-equivalence ratio distributions at (a) 10, (b) 30, (c) 50 and (d) 70 CAD ATDC for regions where the SO_2 to SO_3 conversion is significant.

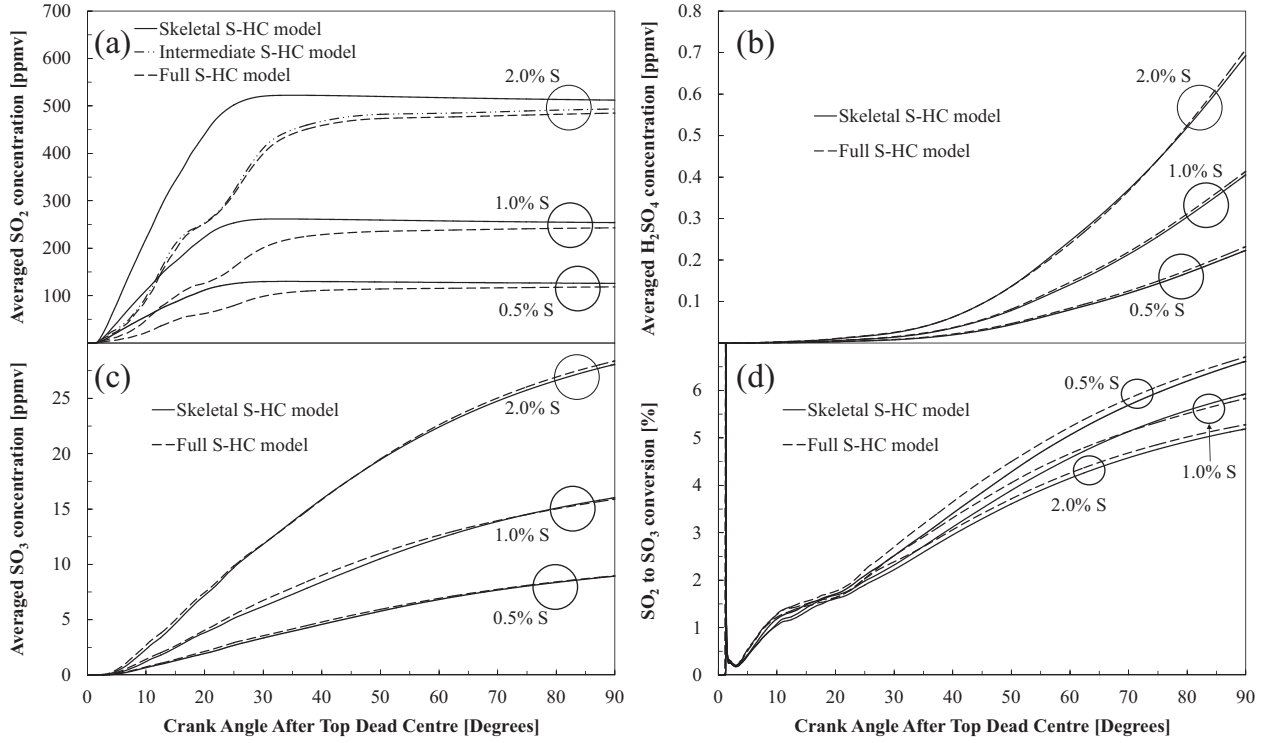

Fig. 7. Temporal evolution of the (a) averaged SO_2 concentrations, (b) averaged SO_3 concentrations, (c) averaged H_2SO_4 concentrations and (d) SO_2 to SO_3 conversion for fuel sulphur contents of 0.5%, 1.0% and 2.0% by mass.

Despite of the difference in SO_2 prediction, Fig. 7(b) shows that the averaged SO_3 concentrations calculated using the skeletal S-HC model are close to those of the base mechanism for all fuel sulphur levels. SO_3 formation is relatively slow and favoured only when the temperature decreases during cylinder expansion. It takes approximately 70 CAD to reach 90% of the final conversion level. Due to the accurate prediction of the SO_3 profiles, the averaged H_2SO_4 concentrations are also reproduced using the skeletal S-HC model. Fig. 7(d) shows the conversion for the three fuel sulphur contents. When the skeletal model is used, Eq. (1) is used to compute the conversion factor. As the full model is utilised, a certain amount of H_2S is predicted in the early stage and its concentration is taken into consideration. As seen, the final conversion factors vary within a range of 5.0–6.5%. The conversion from SO_2 to SO_3 depends on the availability of free radicals, mainly atomic O. When the fuel sulphur content is low relative to the fuel amount, there are more radicals available. The conversion hence increases inversely with the fuel sulphur content. This agrees qualitatively with experimental results presented by Engel et al. [11].

3.2.3. SO_2 and H_2SO_4 formation on cylinder liners

The full and skeletal S-HC mechanisms are next used to predict SO_2 and H_2SO_4 concentrations on the cylinder liner. Fig. 8(a) shows that the maximum SO_2 mass fraction at the cylinder liner calculated using the skeletal S-HC model is approximately 0.004 which is about 1.5-fold higher than that predicted using the base counterpart. As discussed earlier, the difference is attributed to the H_2S which is formed within the fuel rich region but is yet to be oxidised to SO_2. On the other hand, Fig. 8(b) displays that the maximum H_2SO_4 mass fraction predicted by both the S-HC mechanisms has no significant difference. Subsequently, effects of the wall temperature on SO_2 and H_2SO_4 formation at the wall liner are investigated. The liner wall temperature is increased from 323 K to 523 K, in which the latter is the maximum temperature measured in this marine test engine [32]. When the wall temperature is increased to 523 K, the maximum H_2SO_4 mass fraction is marginally lower and the averaged H_2SO_4 concentration at 90 CAD ATDC is reduced by 0.2 ppmv.

This section demonstrates that the skeletal S-HC model is capable of replicating the important characteristics in SO_x formation. With the use of four 64-bit Intel Ivy Bridge Xeon E5-2650 v2 8-core CPUs running at 2.60 GHz [34], the computational runtime consumed by the skeletal S-HC mechanism is approximately 160 hours, which is 1.8-fold shorter than that of the full S-HC mechanism. This indicates that implementation of the skeletal model achieves a good compromise between accuracy and computational efficiency. The numerical model is next evaluated through a parametric study at different engine operating conditions.

3.3. Model evaluation

3.3.1. Parametric study under the full load condition

All the simulations presented in this section are carried out at a fuel sulphur content of 2.0% by mass while the liner wall temperature is fixed at 323 K. The maximum tangential velocity is first varied. This serves to study the influence of different swirl velocity levels in the combustion chamber. Fig. 9(a)(i) shows that the peak pressure is lower by approximately 5 bar when the maximum tangential velocity is reduced from 26 m/s to 16 m/s. In these test cases, the SO_2 formation is similar. As seen in Fig. 9(a)(ii), the onsets of SO_2 to SO_3 conversion are the same for three cases but the conversion in the low swirl case starts to diverge at approximately 15 CAD ATDC. The top view of resampled volume of O radicals at 10 CAD ATDC is provided in Fig. 10 to elucidate the phenomena. The outline of Fig. 10 represents the edge of the cylinder, while the centreline is the cyclic boundary where the 180° domain is revolved to full cylinder to illustrate the in-cylinder event. It is apparent that the flame is more rapidly transported by the stronger swirling flow in the high swirl cases. A greater amount of O radicals are entrained into the flame jet at the opposite side. The earlier flame interaction allows the O atoms to react earlier with SO_2, promoting a higher level of SO_2 to SO_3 conversion. For all the cases, the swirling flow weakens in the later phase of the expansion stroke. The turbulence intensity and hence the mixing rate reduce correspondingly. The conversion remains lower in the low swirl case, as illustrated in Fig. 9(a)(ii). It should also be highlighted that the micro-mixing at molecular level is not considered here since the WSR model is applied in the current simulations. Yet, this trend somewhat agrees with the multi-zone results presented by Cordtz et al. [5], which showed a decrease in SO_3 level when the gas mixing constant is reduced.

The second parameter investigated is the SOI timing. The SOI timing is advanced to TDC and retarded to 2.4 CAD ATDC, while keeping the injection duration, the mass flow rate and the fuel amount unchanged. In the SOI sweep, the in-cylinder temperatures at SOI in these test cases are similar due to the minor variation. Also, since the adiabatic flame temperature (T_{ad}) is not significantly influenced by the in-cylinder pressure [19], both the peak and mean T_{ad} values in these cases are identical. Fig. 9(b)(i) depicts that the SOC is delayed with the SOI. Corresponding to this, the associated temperature increases at a later CAD and the peak pressure drops. As it may be expected, the onset of SO_2 is delayed with the SOI. Since the oxidation of fuel-S to SO_2 is a fast reaction, the averaged concentration eventually increases to a similar level to that of the early injection case. However, the associated SO_2 goes through the oxidation process later in the retarded injection cases. As a result, the SO_2 to SO_3 conversion at

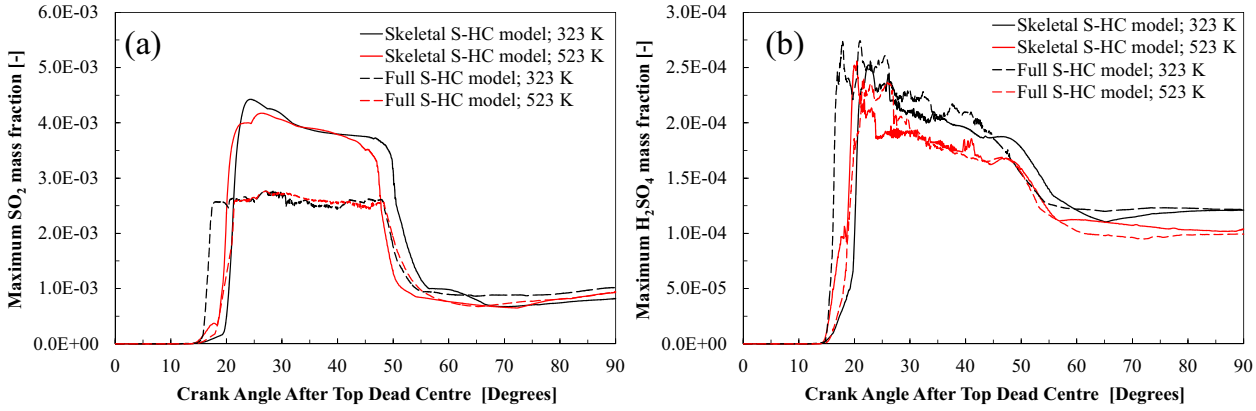

Fig. 8. Temporal evolution of the maximum (a) SO_2 and (b) H_2SO_4 mass fraction at the liner wall calculated using different chemical mechanisms and wall temperatures.

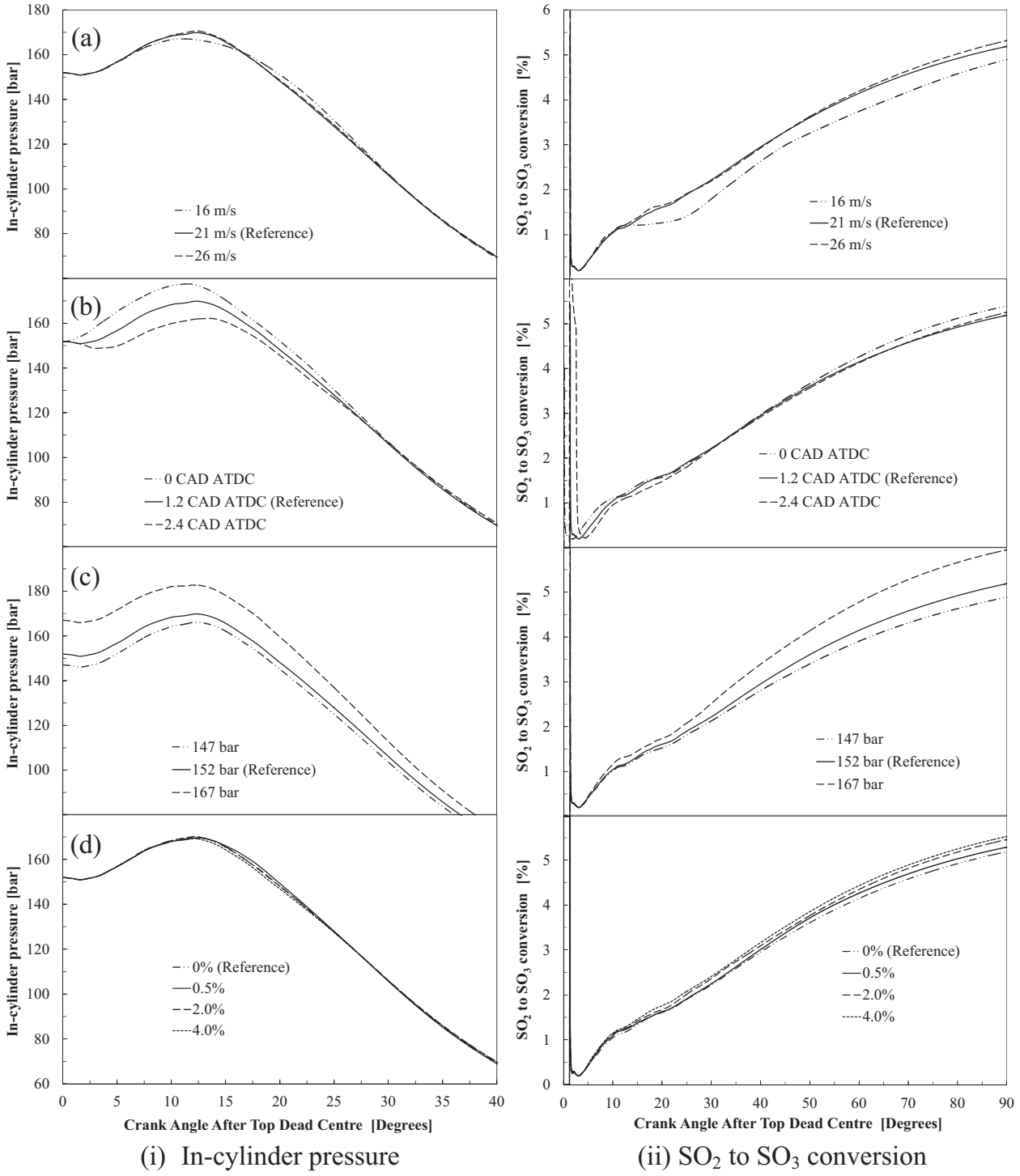

Fig. 9. Comparisons of (i) averaged in-cylinder pressure and (ii) SO_2 to SO_3 conversion for different (a) swirl velocity, (b) start of injection timing, (c) pressure at TDC as well as (d) initial H_2O mass fraction.

90 CAD ATDC drops when the SOI timing is delayed. This is depicted in Fig. 9(b)(ii). The same trend is observed in the measurements performed by Cordtz et al. [10] in the medium speed four-stroke engine.

The in-cylinder P_{TDC} is varied next, with the aim to emulate a change of scavenge pressure. Fig. 9(c)(i) shows that the peak pressures are lower at decreased in-cylinder pressures but the SOC in these cases are identical due to such high pressure conditions. As aforementioned, the peak T_{ad} is not strongly affected by the in-cylinder pressure at SOI. It is also noticed that the flame interaction begins at a similar CAD. Hence, it is deduced that the in-cylinder air mass plays an important role in determining the SO_2 to SO_3 conversion here. As the trapped air mass is reduced in the lower P_{TDC} but the total amount of fuel delivered remains the same, the associated global air to fuel ratio decreases. As a consequence, the formation rates of SO_3 and the associated conversion decrease. This variation, as seen in Fig. 9(c)(ii), agrees qualitatively with the measurements reported by Cordtz et al. [10].

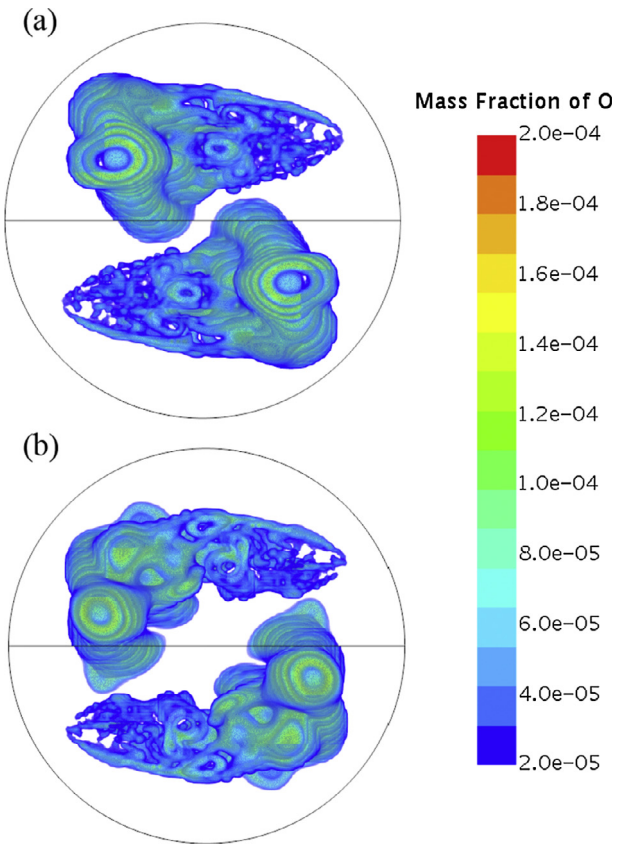

Fig. 10. Comparisons of atomic oxygen (O) evolutions in the (a) $U_{0,max}$ = 16 m/s and (b) $U_{0,max}$ = 26 m/s cases.

The last parameter varied is the initial H_2O level. 0.5%, 2.0% and 4.0% of H_2O (by mass) is introduced in the initial condition while the O_2 concentration is kept unchanged. As shown in Fig. 9(d)(i), the peak pressure levels in all four cases do not vary. The SOC, flame interaction timing and in-cylinder air mass are also identical. Nonetheless, the presence of the water vapour increases the O/H radical pool that promotes the SO_2 oxidation. The averaged OH concentration is found to increase with the increase of initial H_2O levels. Under these conditions, SO_3 is formed mainly by the sequence through reactions 4 and then 5 in their forward direction [16]. As a result, the SO_2 to SO_3 conversion increases with the humidity.

To date, SO_2 to SO_3 conversion measurements under the full load condition is not available. However, the simulation results presented in this section demonstrate that the variation of the conversion with respect to the change of operating parameters predicted by the CFD-chemical kinetic model qualitatively agrees with numerical and experimental results from the literature [5,10,11,16]. The model is next applied to simulate the SO_2 to SO_3 conversion under the low load condition. The simulated results are compared against the measurements obtained from the same research engine.

3.3.2. Comparison with engine measurements under low load condition

As shown in Fig. 11(a), the peak pressures in both of the low load cases are captured, although a maximum relative difference of 6.2% is observed in terms of peak pressure. In the experiments, the salt method was used to analyse the SO_3/H_2SO_4 content in the exhaust gas [35,36]. This was then used to calculate the conversion levels. Eleven measurements were carried out for the low load, low scavenge pressure case. The conversion varies within a narrow range of 4.2–4.7%, showing that the reproducibility of the salt method is acceptable. When the salt method was used for the low load, high scavenge pressure case, a higher conversion level of 5.4% was recorded. These values are plotted in Fig. 11(b) for comparison purposes. It is found that the experimental trend is reproduced by the model as well, even though the predicted conversion levels are consistently higher.

As the engine operates at different loads, the in-cylinder pressure, engine speed and total amount of fuel delivered are varied. Variation of these parameters has opposite effects on the overall conversion [5,10]. The competing effects among these parameters is investigated by converting the full load (reference) case to the low load, high scavenge pressure case in a step–wise manner (not shown). It should be mentioned that this parametric study is solely used to examine the competing effects among the engine parameters on the conversion and these intermediate operating conditions are not feasible in the test engine. At the lower engine load, the in-cylinder pressure is lower and hence the SO_2 to SO_3 conversion decreases. By reducing the in-cylinder pressure by a factor of two (from 152 bar to 76 bar), the conversion level at 90 CAD ATDC is decreased by a factor of four. Apart from the in-cylinder pressure, the engine speed also reduces to 78 rev/min in the low load case. A longer period is available for gas mixing, promoting the SO_2 to SO_3 conversion. The effect of the engine speed, however, is less pronounced. An increase by approximately 0.32 percentage point is observed when the engine speed is reduced from 123 to 78 rev/min. Lastly, the total fuel amount delivered is reduced by approximately 50% in the low load case as compared to that under the full load condition. This increases the global air to fuel ratio and consequently increases the conversion level by a factor of four. As the total fuel amount delivered is scaled with in-cylinder air mass, the global fuel to air ratio becomes similar. The resulting conversions for low and full load conditions do not vary significantly. A one percentage point increase is observed for the estimated conversion at 90 CAD in the low load, high scavenge pressure case. The simulated averaged SO_x/H_2SO_4 concentrations at 90 CAD ATDC for all the test cases are summarised in Table 5.

3.4. In-cylinder phenomena

The temporal evolution of SO_x and H_2SO_4 mass fractions at the liner wall under the low load, low scavenge pressure condition are investigated. In this case, the flame impingement starts at 6 CAD ATDC and small patches of H_2SO_4 are observed on the cylinder liner surface. The flue gas correlation as expressed by Eq. (2) is used to estimate the dew point temperature, T_{DP} (in the unit of Kelvin) and to assess the possibility of acid condensation.

$$T_{DP} = [2.276 \times 10^{-3} - 2.943 \times 10^{-5}(lnp_{H_2O}) - 8.58 \times 10^{-5}(lnp_{H_2SO_4}) + 6.2 \times 10^{-7}(lnp_{H_2O})(lnp_{H_2SO_4})]^{-1} \quad (2)$$

p in Eq. (2) is the partial pressure in millimetre in mercury (mmHg) of each participating species [37].

As shown in Fig. 12(a), the highest dew point temperature appears to be 502 K at 6 CAD ATDC for the current case. This indicates that the acid condensation may start early at the upper part of the cylinder liner. The results are consistent with practical experience of large two-stroke engines where corrosion-induced wear is pronounced in the top of the liner around the ring pack position at TDC [38]. The region with high dew point temperatures becomes broader at 10 CAD ATDC and its distribution covers majority of the engine liner at 15 CAD ATDC. These distributions are illustrated in Fig. 12(b) and (c), respectively.

Scatter plots of the H_2SO_4 molar concentration against the distance from the wall are constructed for gas with different

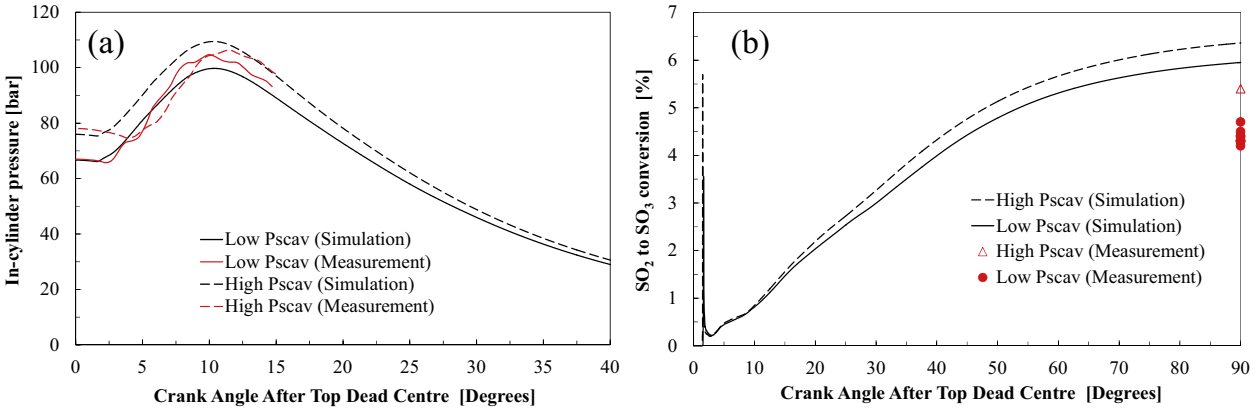

Fig. 11. Comparisons of (a) averaged in-cylinder pressure and (b) SO_2 to SO_3 conversion for the low load, high scavenge pressure case and the low load, low scavenge pressure case.

Table 5
Averaged SO_x/H_2SO_4 concentrations at 90 CAD ATDC in all the test cases.

Engine parameters	Species concentrations [ppmv]		
	SO_2	SO_3	H_2SO_4
Fuel sulphur (% by mass)			
0.5	125.9	8.9	0.2
1.0	254.0	16.0	0.4
2.0	512.2	28.1	0.7
$U_{i,max}$ (m/s)			
16	514.5	26.5	0.6
21	512.2	28.1	0.7
26	510.9	28.7	0.7
SOI ATDC (CA°)			
0	510.8	29.2	0.7
1.2	512.2	28.1	0.7
2.4	512.9	28.5	0.6
Initial H_2O (% by mass)			
0	512.2	28.1	0.7
0.5	511.1	28.6	0.9
2.0	510.2	29.5	1.2
4.0	509.4	29.9	1.6
P_{TDC} (bar)			
147	529.5	27.3	0.7
152	512.2	28.1	0.7
167	463.4	29.3	1.0
67[a]	455.1	28.9	1.1
76[a]	433.0	29.5	1.1

[a] Low load cases.

temperature ranges. These plots are provided in Fig. 13 and are used to inspect the H_2SO_4 boundary layer. At 15 CAD ATDC, the in-cylinder temperature is still high and the temperature gradient is steep towards the cylinder wall. For instance, at the Point A indicated in Fig. 12(c), a variation of approximately 2000 K is observed within a distance of 0.2 mm. The formation of H_2SO_4 is hence very close to the wall where the temperature is low. The reaction zone has a thickness of approximately 0.02 mm and the production rate significantly falls at temperatures above 600 K (not shown). At this CAD, the gas containing high H_2SO_4 molar concentration is mainly observed in the region 0.1 mm from the wall. It appears to be approximately fivefold thicker than the region where H_2SO_4 is produced, suggesting that the H_2SO_4 boundary layer thickness is influenced by convection. At the later CADs, the in-cylinder temperature reduces due to volume expansion. The local temperature at the region adjacent to the wall decreases correspondingly and the H_2SO_4 boundary layer thickness increases since these low temperature regions favour for H_2SO_4. The scatter plots given in Fig. 13(b)–(d) are used to illustrate the development of the boundary layer during the expansion stroke.

On the other hand, a noticeable amount of SO_2 has yet to be converted to SO_3 and reaches the cylinder liner. This is similar to the previous observation in the high load case as discussed in Section 3.2.3. Under the low load condition, SO_2 appears at the liner at 6 CAD ATDC alongside the flame impingement (not shown). The SO_2 distribution becomes broad at 15 CAD ATDC and it lasts until approximately 25 CAD ATDC. During this period, SO_2 may absorb into the engine lubricating oil film and potentially contribute to cylinder wear [1].

The numerical model, which has been developed and evaluated in the present work, is expected to serve as an important prerequisite for further studies related to the corrosion-induced wear phenomenon in the large two stroke marine engines. For instance, together with a fluid film model, the H_2SO_4 condensation rate on the lube oil film and the associated condensed mass can be investigated [39]. Similarly, the investigation of the SO_2 absorption rate into the engine lube oil film on the cylinder liner can also be carried out. An improved understanding of these processes is crucial to address the corrosion-induced wear issue and hence to prolong the marine engine lifespan with minimal expenses on lubrication.

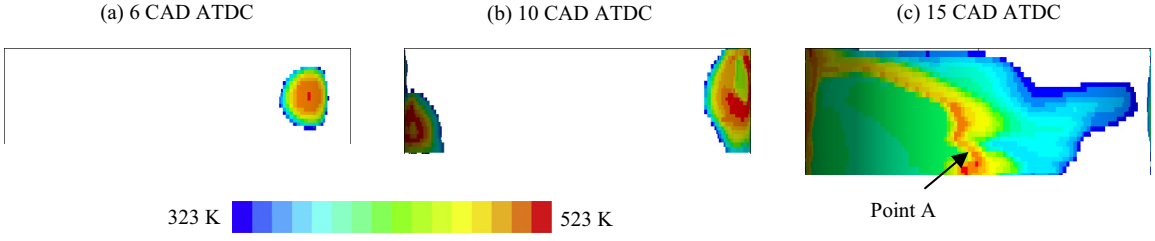

Fig. 12. Spatial distributions of the calculated dew point temperature on cylinder liner at (a) 6, (b) 10 and (c) 15 CAD ATDC.

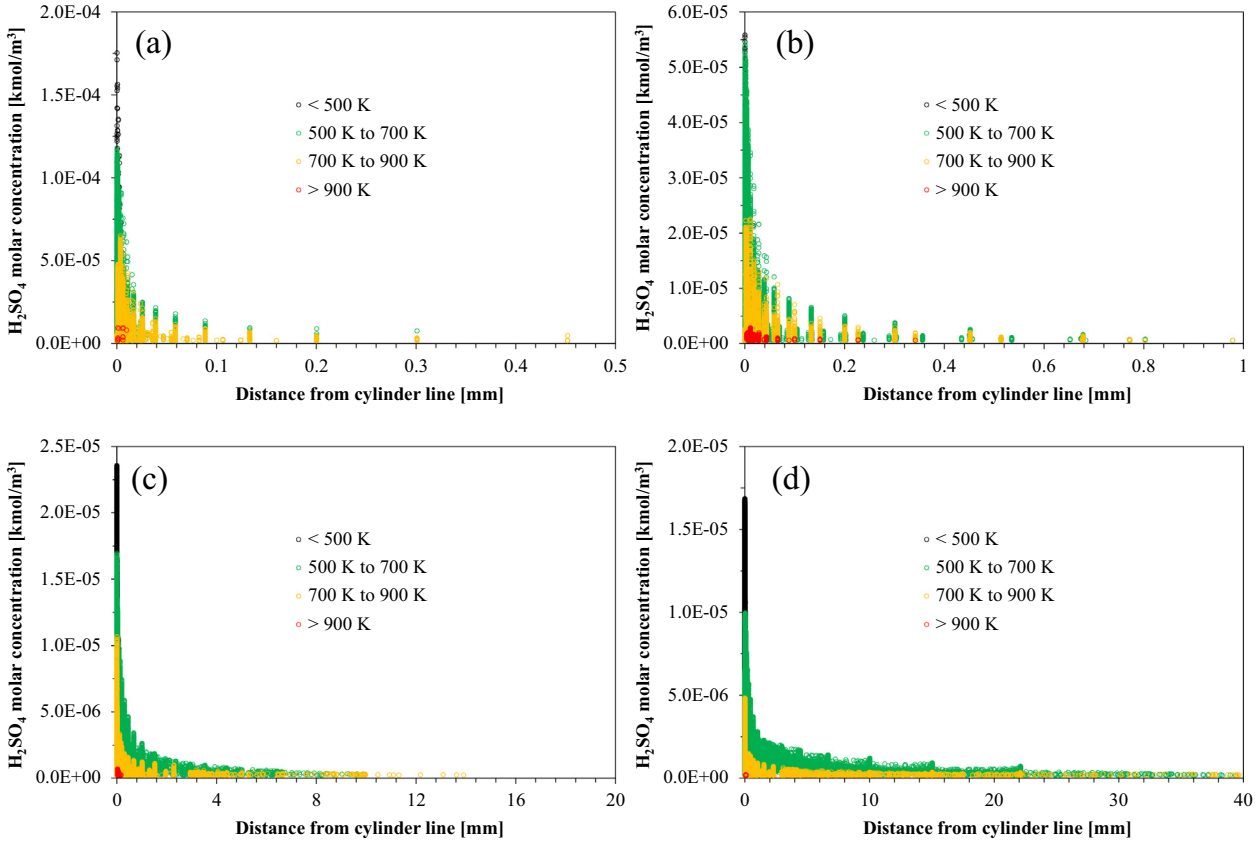

Fig. 13. Local H_2SO_4 molar concentration at (a) 15, (b) 30, (c) 45 and (d) 60 CAD ATDC. The computational cells are grouped based on the local gas temperature.

4. Conclusions

This work presents 3-D CFD modelling of SO_x and H_2SO_4 formation in the HFO combustion under the large, low speed two-stroke marine diesel engine-like conditions. A HFO surrogate model, namely skeletal S-HC mechanism is constructed by integrating a reduced sulphur mechanism and a skeletal *n*-heptane mechanism. The final surrogate fuel model which considers fuel and small hydrocarbon oxidation, thermal NO production as well as SO_x and H_2SO_4 formation consists of 37 species and 77 reactions. It is shown in the current work that although the associated averaged SO_2 concentration at 90 CAD ATDC is higher than that predicted using its base counterpart, the maximum relative difference remains within 6%. Besides this, the predicted temporal evolution of SO_3 and H_2SO_4 using both mechanisms are identical. With the use of the skeletal S-HC model, the following conclusions can be drawn:

- Variation of the conversion in response to the change of fuel sulphur content, swirl velocity, SOI timing, scavenge pressure, humidity and engine load estimated by the model is in good qualitative agreement with the numerical and experimental results from the literature.
- The key factor influencing the difference in high and low load cases is the global air to fuel ratio which depends on the in-cylinder mass of the trapped air and the total fuel amount delivered.
- The simulated SO_2 to SO_3 conversion levels under the low load conditions are close to the measurements recorded from the same marine engine.
- Acid condensation could begin at approximately 6 CAD ATDC when the flame hits the top part of the engine liner, corresponding well with the distribution of corroded parts observed in the engine cylinder.
- Relatively large amount of SO_2 are also found to dwell at the cylinder liner, suggesting that SO_2 may absorb into the engine lubricating oil film and potentially contribute to cylinder wear.

Acknowledgements

The authors gratefully acknowledge funding from the Innovation Fund Denmark and MAN Diesel & Turbo A/S through the SULCOR project. The authors also thank Henrik Christensen, Julia Svensson, Mark Hoffmann and Dorthe Jacobsen from MAN Diesel & Turbo SE for preparing the experimental data.

References

[1] Nagaki H, Korematsu K. Effect of sulfur dioxide added to induction air on wear of diesel engine. SAE technical paper 930994; 1993.
[2] Glarborg P, Kubel D, Dam-Johansen K, Chiang HM, Bozzelli JW. Impact of SO_2 and NO on CO oxidation under post-flame conditions. Int J Chem Kinet 1996;28:773–90.
[3] Sautermeister FA, Priest M. Physical and chemical impact of sulphuric acid on cylinder lubrication for large 2-stroke marine diesel engines. Tribol Lett 2012;47:261–71.
[4] Sautermeister FA, Priest M, Lee PM, Fox MF. Impact of sulphuric acid on cylinder lubrication for large 2-stroke marine diesel engines: contact angle, interfacial tension and chemical interaction. Tribol Int 2013;59:47–56.
[5] Cordtz R, Schramm J, Andreasen A, Eskildsen SS, Mayer S. Modeling the distribution of sulfur compounds in a large two stroke diesel engine. Energy Fuels 2013;27:1652–60.
[6] Imperato M, Kaario O, Sarjovaara T, Larmi M. Split fuel injection and Miller cycle in a large-bore engine. Appl Energy 2016;162:289–97.
[7] Ryu Y, Lee Y, Nam J. Performance and emission characteristics of additives-enhanced heavy fuel oil in large two-stroke marine diesel engine. Fuel 2016;182:850–6.
[8] Kasper A, Aufdenblatten S, Forss A, Mohr M, Burtscher H. Particulate emissions from a low-speed marine diesel engine. Aerosol Sci Technol 2007;41:24–32.

[9] Tsukamoto T, Ohe K, Okada H. Particulate emissions from a two-stroke marine diesel engine operated with heavy fuel oil. In: ICE-Vol. 39, design, application, performance and emissions of modern internal combustion engine systems and components. ASME; 2002 [ICEF2002-503].
[10] Cordtz R, Schramm J, Rabe R. Investigating SO_3 formation from the combustion of heavy fuel oil in a four-stroke medium speed test engine. Energy Fuels 2013;27:6279–86.
[11] Engel PK, Thompson RE, Silvestrini R. Corrosion and fouling potential in diesel exhausts. J Eng Power 1979;101:598–606.
[12] Andreasen A, Mayer S. Modelling of the oxidation of fuel sulfur in low speed two-stroke diesel engines. CIMAC paper no. 39; 2010.
[13] Merryman EL, Levy A. Kinetics of sulfur-oxide formation in flames: II. Low pressure H2S flames. J Air Pollut Contr Assoc 1967;17:800–6.
[14] Muller CH, Schofield K, Steinberg M, Broida HP. Sulfur chemistry in flames. Symp Combust 1979;17:867–79.
[15] Zachariah MR, Smith OI. Experimental and numerical studies of sulfur chemistry in $H_2/O_2/SO_2$ flames. Combust Flame 1987;69:125–39.
[16] Hindiyarti L, Glarborg P, Marshall P. Reactions of SO_3 with the O/H radical pool under combustion conditions. J Phys Chem A 2007;111:3984–91.
[17] Yilmaz A, Hindiyarti L, Jensen AD, Glarborg P, Marshall P. Thermal dissociation of SO_3 at 1000–1400 K. J Phys Chem A 2006;110:6654–9.
[18] Raptotasios SI, Sakellaridis NF, Papagiannakis RG, Hountalas DT. Application of a multi-zone combustion model to investigate the NO_x reduction potential of two-stroke marine diesel engines using EGR. Appl Energy 2014;157:814–23.
[19] Pang KM, Karvounis N, Walther JH, Schramm J. Numerical investigation of soot formation and oxidation processes under large two-stroke marine diesel engine-like conditions using integrated CFD-chemical kinetics. Appl Energy 2016;169:874–87.
[20] Andreadis P, Zompanakis A, Chryssakis C, Kaiktsis L. Effects of the fuel injection parameters on the performance and emissions formation in a large-bore marine diesel engines. Int J Eng Res 2009;12:14–29.
[21] Cerru FG, Kronenburg A, Lindstedt RP. A systematically reduced reaction mechanism for sulphur oxidation. Proc Combust Inst 2005;30:1227–34.
[22] Craft TJ, Graham LJW, Launder BE. Impinging jet studies for turbulence model assessment – II. An examination of the performance of four turbulence models. Int J Heat Mass Transf 1992;36:2685–97.
[23] Behnia M, Parneix S, Durbin PA. Prediction of heat transfer in an axisymmetric turbulent jet impinging on a flat plate. Int J Heat Mass Transf 1998;41:1845–55.
[24] Jensen MV, Walther JH. Numerical analysis of jet impingement heat transfer at high jet Reynolds number and large temperature difference. Heat Transf Eng 2013;34:801–9.
[25] Reiner T, Arnold F. Laboratory investigations of gaseous sulfuric acid formation via $SO_3 + H_2O + M \rightarrow H_2SO_4 + M$: measurement of the rate constant and product identification. J Chem Phys 1994;101:7399–407.
[26] Lovejoy ER, Hanson DR, Huey LG. Kinetics and products of the gas-phase reaction of SO_3 with water. J Phys Chem 1996;100:19911–6.
[27] Jayne JT, Poschl U, Chen Y, Dai D, Molina LT, Worsnop DR, et al. Pressure and temperature dependence of the gas phase reaction of SO_3 with H_2O and the heterogeneous reaction of SO_3 with H_2O/H_2SO_4 surfaces. J Phys Chem A 1997;101:10000–11.
[28] Reaction Design. CHEMKIN ® software. Release 4.1.1; 2007.
[29] CD-Adapco. STAR-CCM+ ® documentation. Version 10.06; 2015.
[30] Wilcox DC. Turbulence modeling for CFD. 3rd ed. La Canada (CA): DCW Industries Inc.; 2006.
[31] Salvador FJ, Ruiz S, Gimeno J, De la Morena J. Estimation of a suitable Schmidt number range in diesel sprays at high injection pressure. Int J Therm Sci 2011;50:1790–8.
[32] Sigurdsson E, Ingvorsen KM, Jensen MV, Mayer S, Matlok S, Walther JH. Numerical analysis of the scavenge flow and convective heat transfer in large two-stroke marine diesel engines. Appl Energy 2014;123:37–46.
[33] CIMAC Working Group "Marine Lubricants". Guidelines for diesel engine lubrication – lubricating oil degradation. The International Council on Combustion Engines, CIMAC report no. 22; 2004.
[34] Nielsen OH. Niflheim Linux supercomputer cluster. Available at <https://wiki.fysik.dtu.dk/niflheim/> [accessed on 9 January 2017].
[35] Fleig D, Vainio E, Andersson K, Brink A, Johnsson F, Hupa M. Evaluation of SO_3 measurement techniques in air and oxy-fuel combustion. Energy Fuels 2012;26:5537–49.
[36] Vainio E, Fleig D, Brink A, Andersson K, Johnsson F, Hupa M. Experimental evaluation and field application of a salt method for SO_3 measurement in flue gases. Energy Fuels 2013;27:2767–75.
[37] Verhoff FH, Banchero JT. Predicting dew points of flue gases. Chem Eng Process 1974;70:71–2.
[38] Jensen MF, Bøttiger J, Reitz HH, Benzon ME. Simulation of wear characteristics of engine cylinders. Wear 2002;253:1044–56.
[39] Walther JH, Karvounis N, Pang KM. Numerical simulation of condensation of sulfuric acid and water in a large two-stroke marine diesel engine. In: 69th Annual meeting of the APS division of fluid dynamics, November 20–22, 2016; Portland, Oregon, The United States of America.